mater.scichina.com link.springer.com

Published online 14 June 2024 | https://doi.org/10.1007/s40843-024-2945-7
Sci China Mater 2024, 67(8): 2653–2660

A weavable and wearable polymer ultrasonic transducer with a large bandwidth

Junyi Zou[1†], Xingyi Guo[2†], Jiaqi Wu[1], Dongmei Xu[2], Kailiang Xu[2*], Peining Chen[1*], Dean Ta[2] and Huisheng Peng[1*]

ABSTRACT **The rise of Internet of Things technologies has promoted the rapid advancement of wearable health monitoring devices. While medical ultrasound technology holds promise for long-term monitoring to detect critical chronic diseases, current commercial ultrasound probes often lack the flexibility, miniaturization, and comfort necessary for medical wearable devices. To address this gap, we propose a weavable and wearable polymer ultrasonic transducer comprising a matching layer, a backing layer, and a piezoelectric layer. This transducer exhibits a bandwidth of 93%, which is six times that of transducers made from piezoelectric ceramics, and could withstand over 10,000 cycles of bending and twisting deformations. The transducer successfully monitors blood flow velocity and measures vessel thickness in the carotid artery and cardiac vessel, achieving a signal-to-noise ratio comparable to that of commercial probes. Its wideband property, with a bandwidth of 3.68–10.08 MHz, allows for the monitoring of various tissues through frequency adjustment. Furthermore, the weavable ultrasonic transducer in fiber form is seamlessly integrated into breathable textiles for real-time cardiovascular monitoring without compromising comfort.**

Keywords: ultrasonic transducer, flexible, textile, health monitoring

INTRODUCTION

Medical ultrasound is a radiation-free, portable, real-time imaging technology [1–4] used for examining lesions in tissues and organs [5,6]. For example, ultrasound Doppler technology can monitor blood flow speed to diagnose cardiovascular diseases [7–9]. Ultrasonic devices offer the potential for long-term monitoring to effectively prevent and diagnose diseases [10–12]. The rise of Internet of Things technologies has accelerated the rapid development of wearable devices, potentially revolutionizing medical electronics [13–15]. However, current rigid bulk ultrasonic devices are often unsuitable for the inherent requirements of flexibility, miniaturization, and comfort in medical wearables [16–19]. There is an urgent need to develop a new type of ultrasonic device capable of conforming to irregular and soft human body shapes, maintaining stable performance under complex deformations, and ensuring breathability for optimal wearing comfort.

Ultrasonography, a key medical imaging technique with a history spanning approximately 100 years, traces back to the discovery of the piezoelectric effect in quartz crystals (Fig. S1) [20,21]. Piezoelectric ceramics, notably lead zirconate titanate (PZT), have demonstrated excellent electromechanical coupling performances [22–26]. Despite these advancements, the inherent rigidity and bulkiness of traditional ultrasonic devices necessitate the use of liquid or soft coupling gel to conform to varying human body shapes. Efforts to improve flexibility have been explored, including the design of island-bridge-structure piezoelectric ceramics on flexible substrates such as polyimide (PI) or elastomer [10,27–29]. However, these structurally flexible devices are susceptible to failure under certain complex deformations owing to modulus mismatch and potential interface separation at the junction where soft and hard segments meet [17]. Moreover, the thickness (typically larger than 0.2 mm) of PZT ceramics used in these ultrasonic devices generally limits their applications under high frequencies. Therefore, intrinsically flexible ultrasonic devices that can conform well to human bodies still need to be developed.

Here, we introduce a weavable and wearable polymer ultrasonic transducer (PUT) in fiber form, with polyvinylidene fluoride (PVDF) as the piezoelectric layer and polyurethane (PU) and PI as the matching and backing layers. The PUT exhibits a central frequency of 6.88 MHz and an impressive bandwidth of 93%, which is six times broader than transducers based on piezoelectric ceramics. Even after 10,000 cycles of bending and twisting deformations, the normalized amplitude and bandwidth remain stable. The wide bandwidth of the PUT (3.68–10.08 MHz) allows for versatile tissue monitoring through frequency adjustment, facilitating observation of both superficial and deep tissues. Flexible Doppler sensors were successfully developed to monitor blood flow velocity in the carotid artery and heart, with a signal-to-noise ratio (SNR) comparable to that of commercial probes. The PUT fiber can be seamlessly woven into soft and breathable textiles, enabling real-time and wearable cardiovascular monitoring.

[1] State Key Laboratory of Molecular Engineering of Polymers Department of Macromolecular Science, Institute of Fiber Materials and Devices, Laboratory of Advanced Materials, Fudan University, Shanghai 200438, China
[2] Department of Biomedical Engineering, Yiwu Research Institute and Shanghai Poda Medical Technology Co., Ltd., Fudan University, Shanghai 200438, China
[†] These authors contributed equally to this work.
[*] Corresponding authors (emails: peiningc@fudan.edu.cn (Chen P); penghs@fudan.edu.cn (Peng H); xukl@fudan.edu.cn (Xu K))

© Science China Press 2024

EXPERIMENTAL SECTION

Fabrication of PUT

The PUT was fabricated using a poled PVDF film (supplied by ZHIMK Technology (Shenzhen, China) Co., Ltd.) with a thickness of 110 μm as the piezoelectric layer. A 500-nm thick layer of Ag was deposited on both sides of the PVDF through magnetic sputtering. Cu wires, of 50 μm in thickness, were affixed to each side of the film using conductive silver paints (from SPI (West Chester, America) Supplies) as electrodes. The backing layer was constructed using a 100-μm thick PI sheet, onto which a 1-μm thick layer of Cu was deposited on the back side as a shielding layer. A 50-μm thick layer of PU was applied as the matching layer. The various layers of the PUT were adhered together using a 10-μm thick tape. Finally, the PUT was sealed with waterproof super glue M540 (supplied by Sheng Mei Electronic Technology (Taizhou, China) Co., Ltd.).

Fabrication of phantom

Agarose, constituting 2.5% of the weight of distilled water heated to 95°C, was stirred into the solution. Subsequently, the solution was poured into a mold and allowed to cool at room temperature for 10 h. The resulting phantom was then shaped according to specific requirements. PVC powder was introduced into the water at a weight ratio of 1:100. A variable frequency water pump and an LZB-25 fluid flowmeter (supplied by Mont Instrument (Shanghai, China) Co., Ltd.) were employed to regulate the water flow velocity.

Performance measurements of the PUT

Two PUTs were affixed to a 1-cm thick agarose substrate. A sinusoidal voltage of 60 Vpp or pulse voltage was applied to the PUTs using a signal generator (DG4062, RIGOL (Beijing, China) Co., Ltd.) and a wideband amplifier (ATA-1220D, Aigtek (Xi'an, China) Co., Ltd.). The received ultrasonic waves were recorded using an oscilloscope (PicoScope 4824A, Pico Technology (Wales, UK)) equipped with software (PicoScope). Impedance spectroscopy was conducted using a vector network analyzer (Bode 100, Omicron Lab (Salzburg, Austria)). Bending and twisting tests were performed using a custom-made testing apparatus. Temperature measurements were taken using an infrared thermal imager (Optris (Shenzhen, China) PI) in conjunction with analysis software (Optris PIX Connect). The PZT and its composites were sourced from Shen Lei Ultrasonic Instrument (Shaoxing, China) Co., Ltd. and Yi Ying New Material Technology (Shanghai, China) Co., Ltd., respectively.

Performance simulation of PUT

The pulse-echo performances and impedance/phase spectra were simulated using PiezoCAD. The model comprised a 50-μm

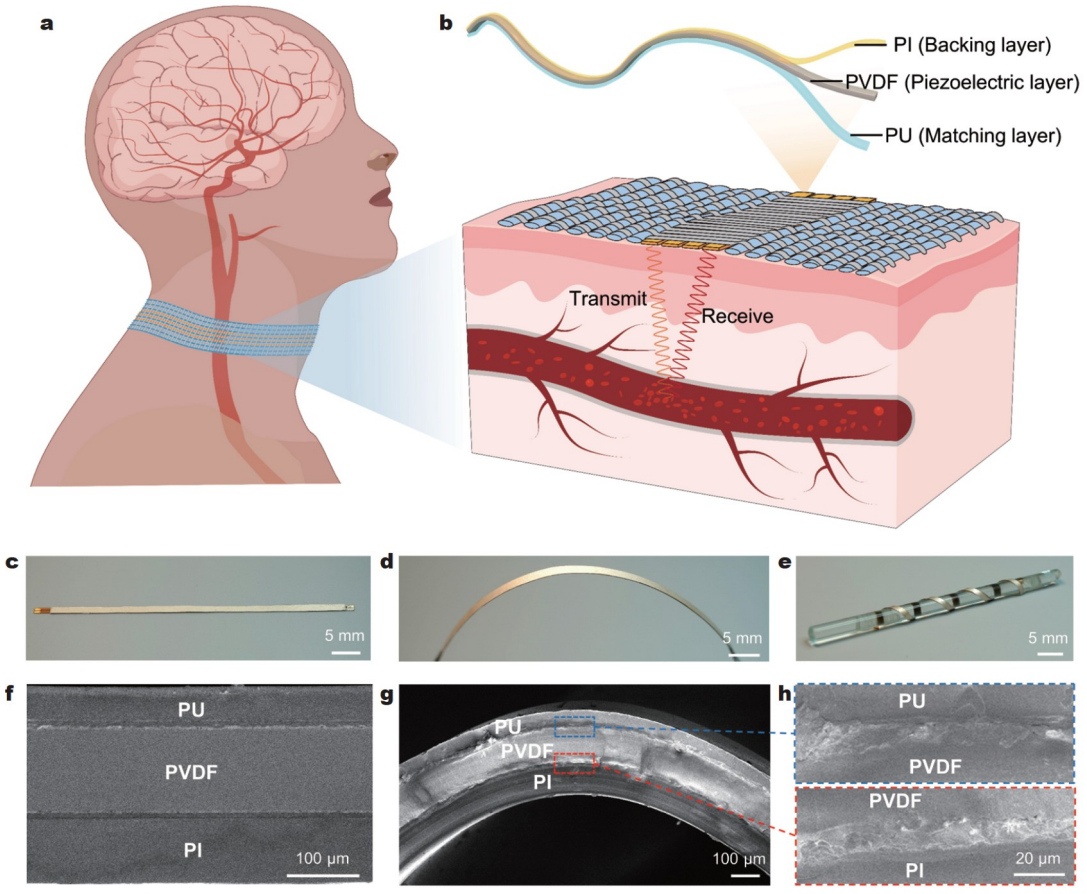

Figure 1 Schematic of the design and working principle of the PUT. (a) Schematic of the fiber PUT woven into textile, illustrating its application scenario. Transducers located on the left and right sides transmit and receive acoustic signals, respectively. (b) Structure of the PUT, comprising matching layer, piezoelectric layer, and backing layer. (c) Photograph of a PUT. Photographs of the PUT under (d) bending and (e) twisting conditions. (f) Scanning electron microscopy (SEM) image of the cross section of the PUT. (g) SEM image of the cross section of the PUT under bending. (h) Enlarged view of the interfaces between PU and PVDF (above) and PVDF and PI (below). No significant interfacial separation occurred between the layers.

© Science China Press 2024

thick PU layer, a 110-μm thick PVDF layer, and a 100-μm thick PI layer.

Blood velocity measurements

PUTs were positioned on the skin around the neck or near the heart, and a coupling agent made of polymer gel (supplied by Cui Mao Instrument (Hangzhou, China) Co., Ltd.) was used to fill the space between the transducer and the skin. A continuous wave was transmitted and received by the PUTs. The received signal was amplified using a charge amplifier (HQA-10M-10T, FEMTO (Berlin, Germany) Messtechnik GmbH). Signal processing was conducted using MATLAB R2021b. A confocal ultrasonic probe obtained from Olympus was used as the commercial probe. Experiments on the neck and heart of humans were conducted according to the regulations of the Animal and Human Experimentation Committee of Fudan University. Written informed consent was obtained from a healthy participant affiliated with Fudan University prior to participation in the study.

Measurements of the vascular wall

A PUT was affixed to the surface of bovine vessels of varying thicknesses. The PUT was then connected to an ultrasonic transmitting and receiving instrument (5900PR, Olympus (UK & Ireland)).

Signal processing

The received ultrasound signal underwent initial conversion into a digital signal for processing through an analog-to-digital converter. To prevent aliasing from other noise components, a bandpass filter centered around $f_0 \pm 1$ MHz was applied, where f_0 represents the original frequency of the ultrasonic wave. Subsequently, the preprocessed signal underwent demodulation to extract the Doppler frequency shift using in-phase/quadrature (IQ) demodulation. This involved multiplication by two emission signals with a 90° phase shift between them. As the resulting outputs contained high-frequency components approximately twice the carrier frequency, a subsequent lowpass filter with a cutoff frequency of f_0 was employed. The complex signal IQ was then derived through the combination of the baseband I signal and Q signal as I + iQ, where i represented the imaginary unit. The IQ signal facilitated the differentiation of positive and negative frequency shifts during frequency analysis. Following demodulation, the IQ signal was downsampled to a sampling rate of 20,000 Hz to facilitate subsequent time-frequency analysis. To differentiate signals from blood flows of those originating from slowly moving muscular tissue and vessel walls [30], which possessed different frequencies due to varying speeds, a highpass filter with a cutoff frequency of 300 Hz was applied. Subsequently, the clutter-filtered IQ signal was subjected to simultaneous time and frequency domain analysis through the short-time Fourier transform (STFT) technique. The resulting spectrum depicts the distribution of frequency components at different time points, representing the velocity distribution. The brightness within the spectrum corresponds to the signal intensity at the respective time and frequency.

RESULTS AND DISCUSSION

The fiber-shaped PUT can be woven into flexible and breathable ultrasound textiles (Fig. 1a, b). The PUT primarily comprises

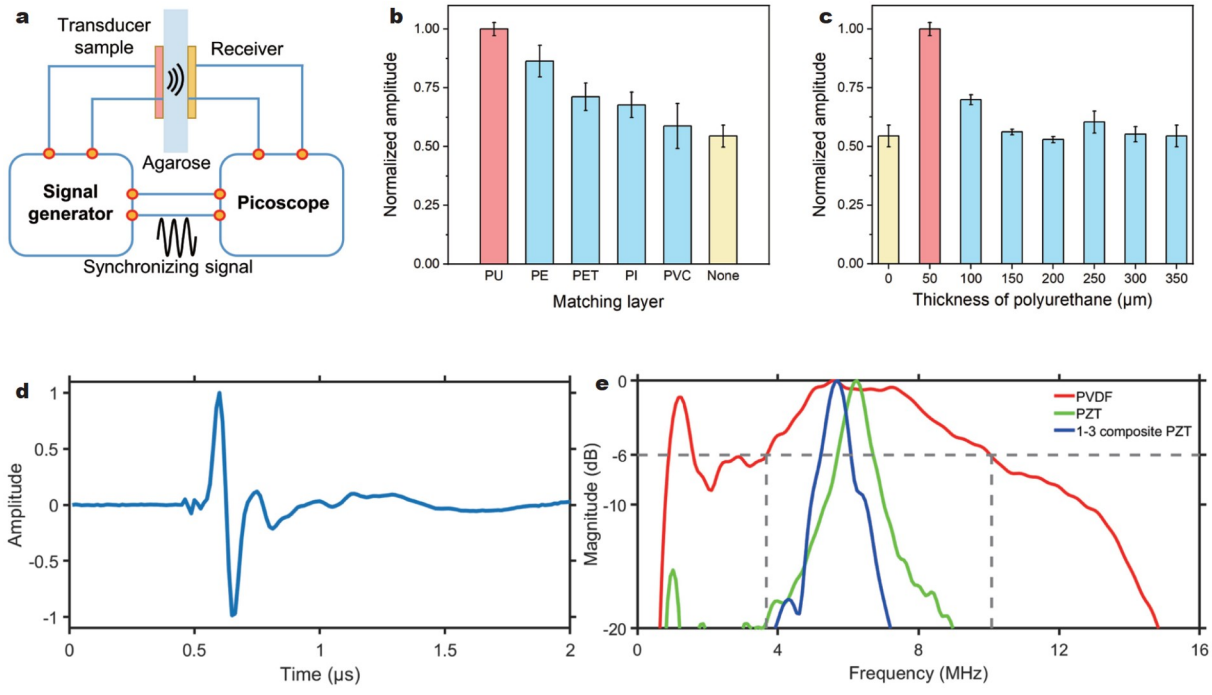

Figure 2 Characterization and optimization of the PUT. (a) Schematic illustrating the principle and process of measuring bandwidth and amplitude of received echoes. Two PUTs were affixed on both sides of a 1-cm thick agarose sample. (b) Normalized amplitude of received waves with varying materials for the matching layer and without a matching layer. Results were normalized against the amplitude obtained with a PU matching layer. (c) Normalized amplitude of received waves with varying thicknesses of PU matching layers. The results were normalized against the amplitude obtained with a 50-μm thickness. (d) Time-domain signal of the received pulse signals. (e) Comparison of bandwidths among PVDF, PZT (with a central frequency of 6.25 MHz), and 1–3 composite PZT (with a central frequency of 5.70 MHz). The bandwidth of our transducer was calculated according to the frequencies ranging from 3.68 to 10.08 MHz.

© Science China Press 2024

three functional layers: The matching layer (PU, 50-μm thick), the piezoelectric layer (PVDF, 110-μm thick), and the backing layer (PI, 100-μm thick) (Fig. 1b, c, f). The PUT, characterized by flexibility and structural stability, can endure deformations such as bending and twisting (Fig. 1d, e). In the bending state, the functional layers maintain close contact with each other (Fig. 1g, h). The matching layer, composed of PU with an acoustic impedance of 2.38 MRayl, ensures ultrasound wave penetration, and its thickness is one-quarter of the ultrasonic wavelength (Note S1). The backing layer was made of PI with a high Young's modulus to enhance the temporal resolution [31]. Furthermore, a 1-μm thick copper (Cu) film was applied to the PI layer surface and grounded to mitigate the impact of electromagnetic waves. As a result, the SNR increased by over 40 dB following the application of the Cu film (Fig. S2), indicating effective electromagnetic wave shielding.

PVDF deposited with Ag electrodes, functioned as the piezoelectric layer responsible for transmitting and receiving ultrasound waves *via* the piezoelectric effect. At a central frequency of 6.88 MHz, the PVDF thickness measured as 110 μm. The electrode connected to the PI layer was designated as the input/output port, while the electrode linked to the PU layer was grounded to enhance electromagnetic shielding further (Note S2). The adhesion layer featured a thickness of 10 μm, approximately one-twentieth of the wavelength (Fig. 1h, Note S1); thus, its impact on sensitivity and flexibility is negligible.

Two PUTs were positioned on both sides of a 1-cm thick agarose sample. The ultrasonic transmission and reception performances were investigated through the application of voltage to one side of the PUTs and the detection of the voltage on the other side (Fig. 2a). A single-frequency ultrasound wave of 10 MHz and 10 cycles were employed to optimize the matching layer (Fig. 2b, c). We assessed the amplitude of the received ultrasound wave with different matching layers, including PU, polyethylene, polyethylene terephthalate, PI, and polyvinyl chloride (Fig. 2b). The PUT without a matching layer was coated with a layer of unpolarized PVDF to ensure waterproofing. The results indicated that the matching layer made of PU, with an acoustic impedance value of 2.38 MRayl, yielded the highest amplitude (Note S1 and Table S1). The PU layer, with a thickness of 50 μm (one-quarter of the 10 MHz ultrasound wave-

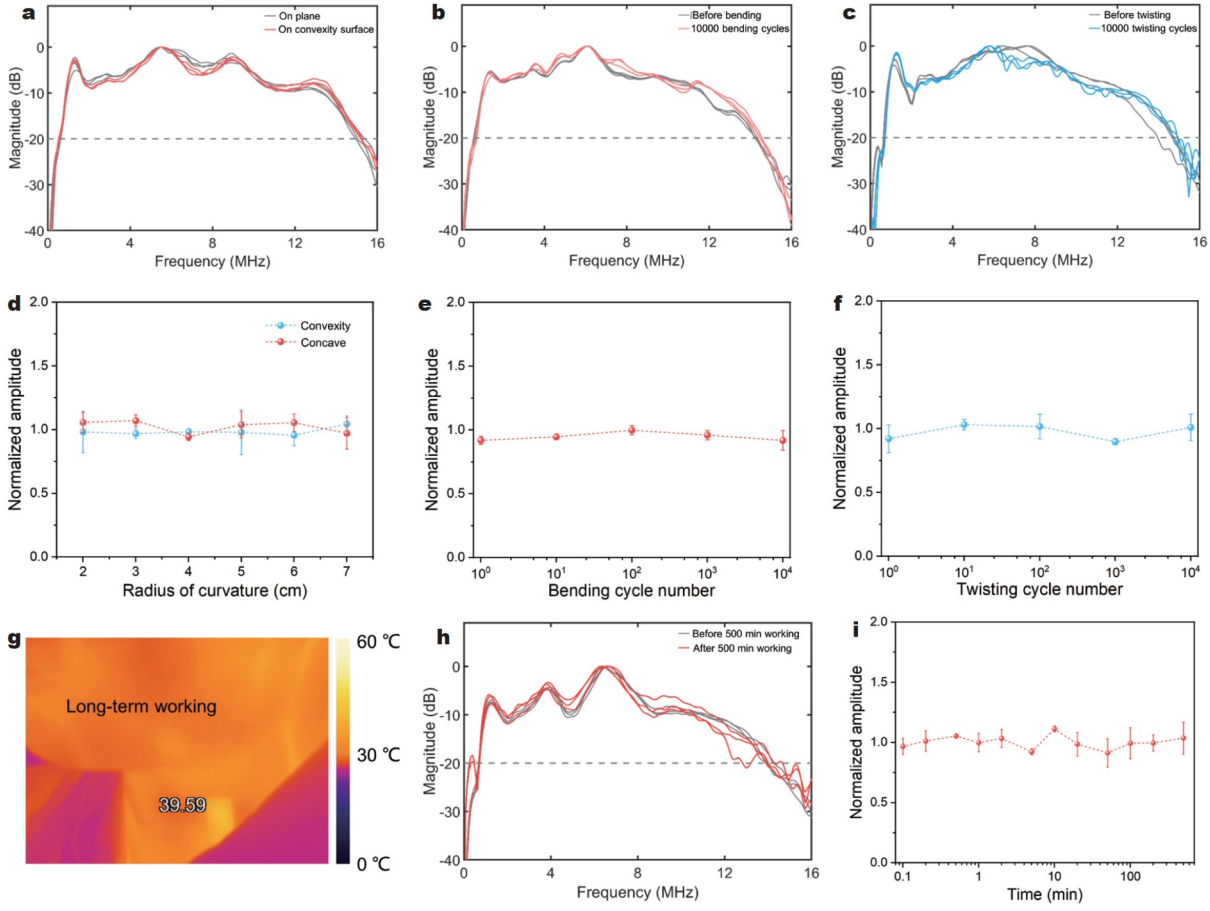

Figure 3 Stability validation of the PUT. (a) Bandwidth measurements when the PUT is attached to the convex surface. (b) Normalized amplitude of the received ultrasonic wave by PUT attached to convex and concave surfaces with various curvature radii. The results were normalized against the data obtained when the PUT was attached to a flat surface. (c) Bandwidth measurements before bending and after the PUT was bent for 10,000 cycles. (d) Normalized amplitude of the received ultrasonic wave before bending and after the PUT was bent for various cycles. The amplitude was normalized against the PUT before bending. (e) Bandwidth measurements before twisting and after the PUT was twisted for 10,000 cycles. (f) Normalized amplitude of the received ultrasonic wave before twisting and after the PUT was twisted for various cycles. The amplitude was normalized against the PUT before twisting. (g) Infrared thermography images of the PUT after continuous 8-h use on the skin. (h) Bandwidth of the PUT before and after 500 min of use. (i) Normalized amplitude of the received ultrasonic wave during use. The amplitude was normalized against the PUT before use.

© Science China Press 2024

length), served as the matching layer and exhibited the highest amplitude (Fig. 2c). Its amplitude was 6 dB higher than that of the PUT without a matching layer. The ideal acoustic impedance for the PVDF matching layer was 2.44 MRayl [32]. The single-layer PU had an acoustic impedance of 2.38 MRayl, which matched well with the acoustic impedance of PVDF [33]. Unless specified otherwise, the PUT with a 50 μm thick PU layer was utilized in the subsequent study.

To confirm the wideband property of the PUT, we generated a pulse wave using one of the PUTs and utilized the other to receive the wave (Fig. 2d). Through Fourier transform analysis, the central frequency was determined to be 6.88 MHz, and the bandwidth (at −6 dB) of the PUT was 93%, ranging from 3.68 to 10.88 MHz. This bandwidth was six times wider than that of transducers made of piezoelectric ceramics (Fig. 2e). Transducers constructed from PZT and its composites exhibited central frequencies of 6.25 and 5.70 MHz, respectively, which were similar to those of our transducers (Table S2). Impedance and phase angle spectroscopy of the PVDF exhibited similarities before and after the manufacturing of the PUT (Fig. S3), suggesting stable maintenance of electromechanical properties. Simulated central frequency and bandwidth were 8.73 MHz and 96% (4.51–12.9 MHz), respectively, aligning closely with experimental results (Fig. S18), and simulated impedance was also in close agreement with measured values (Fig. S19).

Stability is crucial when the PUT is applied to the skin, particularly when it is woven into textiles. The PUT could adapt to various irregular shapes and maintain consistent bandwidth (from approximately 4–10 MHz) and amplitude of the received ultrasonic wave when attached to convex and concave surfaces with various radius curvatures similar to those observed on a flat surface (Fig. 3a, b and Fig. S4). The PUT demonstrated its capability to function effectively on irregular surfaces such as human skin. Even after undergoing 10,000 bending cycles, the bandwidth and amplitude of the received ultrasonic wave remained nearly unchanged (Fig. 3c, d). Stability under complex deformations, such as twisting, is crucial for fiber devices in weaving processes and wearable scenarios. Following 10,000 twisting cycles, the bandwidth and amplitude of the received ultrasonic wave of the PUT remained stable (Fig. 3e, f). The fluctuations observed in the frequency response curves during deformations are attributable to internal stress affecting the frequency response of PVDF. Following continuous operation on the skin for 8 h, the temperature of the PUT did not exceed 40°C (Fig. 3g), while the bandwidth and amplitude of the received ultrasonic wave remained largely unchanged (Fig. 3h, i). The temperature gradually increased with excitation voltage (Fig. S5), yet after continuous operation for 8 h in a 23°C environment, the PUT's temperature did not exceed 31°C, with an increment of less than 10°C (Fig. S6). Interestingly, the amplitude of the received ultrasonic wave in cold air temperatures (below −10°C) was over three times that in 25°C air

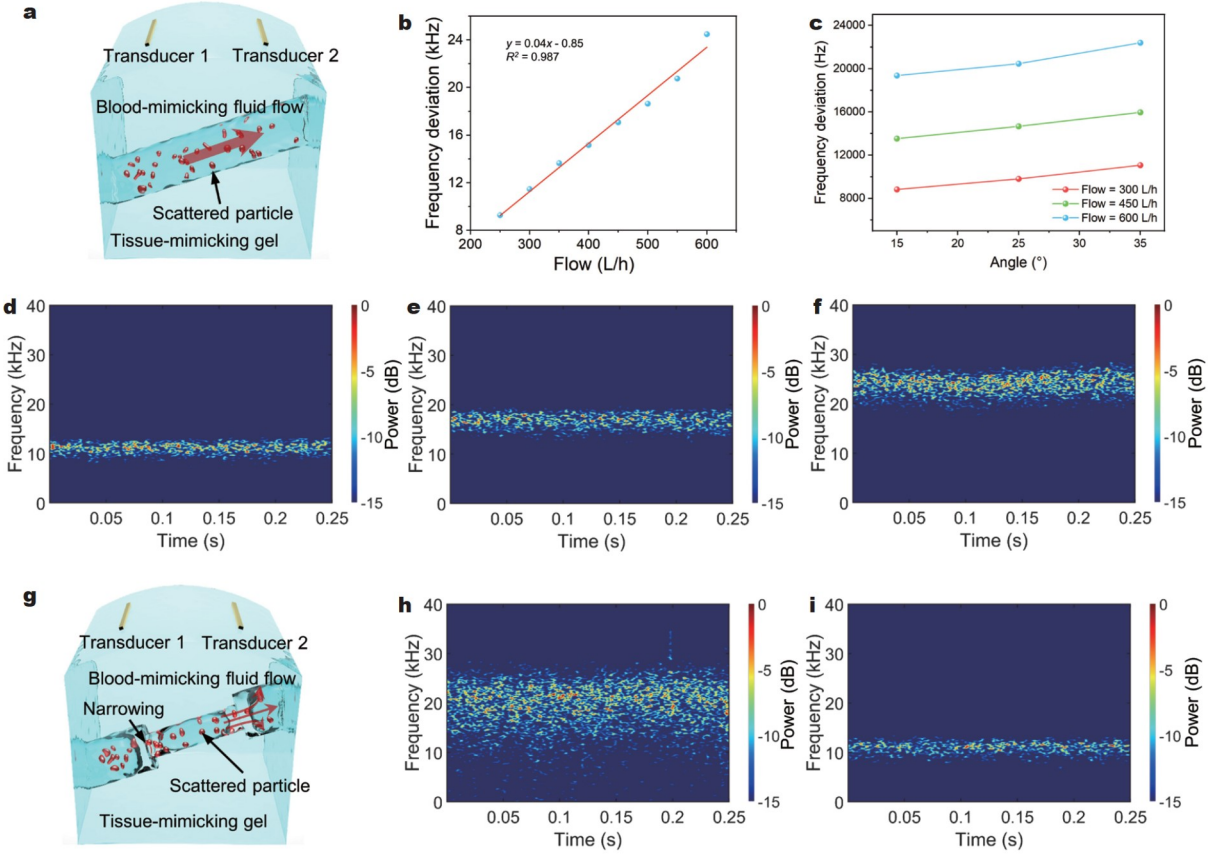

Figure 4 Performance validation *in vitro*. (a) Schematic of the phantom featuring an internal channel. PUTs were attached to the surface. (b) Frequency deviation measurements as flow velocity increased from 250–600 L/h. (c) Frequency deviations at flow velocities of 300, 450, and 600 L/h with PUTs attached at different angles, demonstrating variation with Doppler angle. Velocities of (d) 300, (e) 450, and (f) 600 L/h, allowing for the acquisition of flow velocity distribution. (g) Schematic illustration of the narrowing in the phantom. (h) Time-frequency analysis of the frequency deviation during phantom narrowing. (i) Time-frequency analysis in the case where the PUT was attached to the convex surface of the phantom.

© Science China Press 2024

(Fig. S7). Furthermore, the amplitude of the received ultrasonic wave decreased with increasing temperature above −10°C. These findings demonstrate the PUT's capability to operate effectively in various environments.

Flow velocities were determined according to the ultrasonic Doppler effect (Fig. 1a, Note S3). The Doppler device, comprised of PUTs, emits and receives continuous waves. Continuous wave Doppler is straightforward to operate, involves simple signal processing, and lacks a maximum velocity measurement limit compared to pulse-wave Doppler [34,35]. Erythrocytes, having the same velocity but different acoustic impedance from blood, reflect ultrasonic waves.

The PUT was employed to measure flow speed. The PUT was examined on a blood flow phantom (Fig. 4a) made of agarose with an internal channel. Blood and erythrocytes were simulated using water mixed with polyvinyl chloride powder, while flow velocity was regulated by a pump. Two PUTs were affixed to the phantom, with one transmitting a continuous wave for the other to receive. The results of signal processing indicated that frequency deviation was directly proportional to flow velocity (Fig. 4b, Figs S8, S9). Frequency deviation varied depending on the angle between the two PUTs (Fig. 4c). This bias occurred because the flow velocity (abscissa) represented the average value, while the frequency deviation (ordinate) depicted the peak value. Owing to fluid viscosity, flow velocity near the channel wall was lower than that near the center. The utilization of the STFT process enabled the acquisition of flow velocity distribution variation over time (Fig. 4d–f).

Atherosclerosis or thrombosis can lead to narrowing or complete blockage of arteries, causing a transition from laminar to turbulent flow. To simulate this, we created a narrow channel (Fig. 4g) with a length of 1 cm and a radius of 4 mm. The narrowing increased flow resistance and altered water flow distribution. Consequently, average flow velocity decreased while flow velocity distribution widened (Fig. 4h, Fig. S10). Given the uneven surface of human skin, flow velocity distribution was tested on convex and concave surfaces of the phantom, and the yielding results were consistent with those on a flat surface (Fig. 4i, Fig. S11). This indicates the effectiveness of the PUT on irregular surfaces such as human skin.

Given their easy processing, PUTs can be fabricated into fibers and seamlessly woven into textiles to conform to human skin. Blood flow within vessels is pulsatile and reflects the heartbeat [36], resulting in varying flow velocity (frequency deviation) distributions over time. The carotid artery was chosen for demonstration owing to its straight, thick structure and proximity to the skin surface. During the experiment, a volunteer wore a sweater with fiber PUTs woven into the collar (Fig. 5a). A continuous wave with a single frequency of 10 MHz was utilized. The results revealed a typical blood flow spectrum characterized by five feature points: The first peak systolic velocity (S1), the second systolic velocity (S2), the peak diastolic velocity (D), the end-diastolic velocity (d), and the incisura between systole and diastole (I) (Fig. 5b, Figs S12, S14) [37,38]. The volunteer could hear the frequency deviation as it falls within the audible sound range (Audio S1). This device exhibited a similar performance to

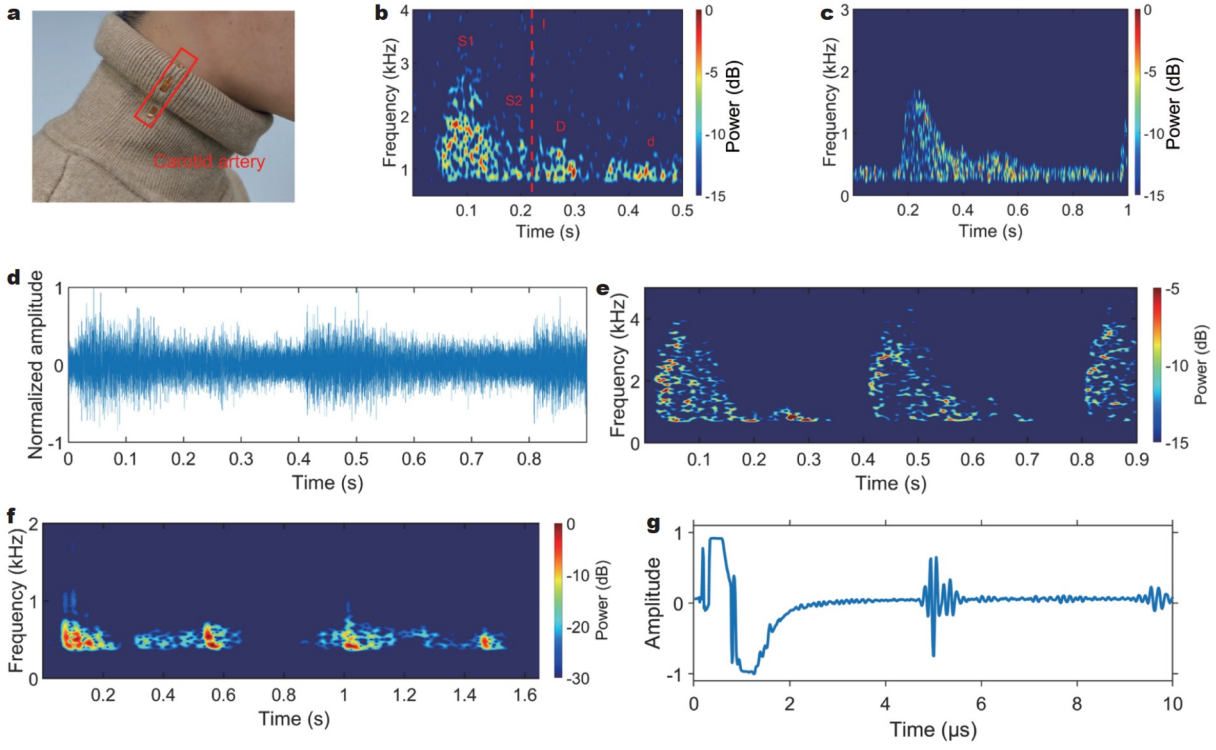

Figure 5 Application presentation of the PUT. (a) Photograph showing the PUT woven into the collar of a sweater. (b) Time-frequency analysis of frequency deviation during measurement of the carotid artery. The transmitted continuous wave has a frequency of 10 MHz, with feature points marked as S1, S2, D, d, and I. (c) Time-frequency analysis of frequency deviation measured using a commercial probe. The transmitted continuous wave exhibited a frequency of 5 MHz. (d) Time-domain signal of frequency deviation of the received continuous wave immediately after a running activity. (e) Time-frequency analysis of frequency deviation immediately after a running activity, showing an increase in both heartbeat frequency and frequency deviation. (f) Time-frequency analysis of frequency deviation of the cardiac vessel. (g) Echo received by the PUT attached to the vascular wall of a bovine vessel with a thickness of 2.75 mm. The first echo appears at 5 μs.

© Science China Press 2024

the commercial ultrasound probe tested on the neck (Fig. 5c).

The PUT is wearable and capable of monitoring long-term flow velocity in the carotid artery on the neck. After the volunteer took a run, the heart rate increased from 60 to 150 beats per minute. Consequently, the blood flow velocity (frequency deviation) noticeably increased, accompanied by changes in distribution (Fig. 5d, e, and Figs S12, S14). Specifically, flow velocity during the systolic process exhibited a significant increase. Subsequently, frequency deviation distribution was assessed after the volunteer rested for 5 min, resulting in corresponding decreases in both heart rate and blood flow velocity (Figs S12–S14).

The cardiac vessel features a considerably more complex vascular path than the carotid artery [39]. Additionally, numerous other vessels adjacent to the cardiac vessel introduce some signal noise. Moreover, the location beneath the skin is deeper, leading to greater attenuation of the ultrasonic wave. Considering the wideband property of PVDF, a 3 MHz ultrasonic continuous wave was employed to minimize sound attenuation in the test. Consequently, although the five feature points might not be distinctly visible, the systolic and diastolic periods were identified (Fig. 5f, and Figs S15, S16). The PUT could monitor different vessels at varying frequencies, owing to its wideband characteristic. Additionally, owing to its high temporal resolution, the PUT could measure the thickness of vascular walls. A pulse wave was transmitted and received by a PUT attached to the surface of a bovine vessel. The thickness of the vessel wall can be determined through the calculation of the time difference between the transmitted and received waves (Fig. 5g and Fig. S17). This highlights the PUT's potential in monitoring vascular wall thickness in implantation scenarios.

CONCLUSIONS

In conclusion, a weavable and wearable PUT with wideband capabilities was successfully developed through the sandwiching of a piezoelectric PVDF layer between PU and PI layers. This polymer-based PUT effectively mitigated module mismatch between its functional layers and thus could endure cyclic deformations such as bending and twisting. Moreover, the device's intricate design, which incorporated matching and shielding layers, addressed the issue of PVDF's weak transmit performance. Shaped as a fiber, the PUT can be seamlessly integrated into textiles, offering excellent wearability and breathability. These features enable noninvasive, long-term, and continuous monitoring applications. The wideband property of the PUT allows for versatile applications, ranging from measurements in high-frequency superficial tissues to low-frequency deep tissues. Blood flow velocity detection and vascular wall measurements were demonstrated in this study.

Received 5 February 2024; accepted 26 April 2024; published online 14 June 2024

1 Hingot V, Brodin C, Lebrun F, *et al.* Early ultrafast ultrasound imaging of cerebral perfusion correlates with ischemic stroke outcomes and responses to treatment in mice. Theranostics, 2020, 10: 7480–7491
2 Provost J, Garofalakis A, Sourdon J, *et al.* Simultaneous positron emission tomography and ultrafast ultrasound for hybrid molecular, anatomical and functional imaging. Nat Biomed Eng, 2018, 2: 85–94
3 Villemain O, Baranger J, Friedberg MK, *et al.* Ultrafast ultrasound imaging in pediatric and adult cardiology. JACC-Cardiovasc Imag, 2020, 13: 1771–1791
4 Wells PNT. Ultrasonic imaging of the human body. Rep Prog Phys, 1999, 62: 671–722
5 Zarins CK, Giddens DP, Bharadvaj BK, *et al.* Carotid bifurcation atherosclerosis. Quantitative correlation of plaque localization with flow velocity profiles and wall shear stress.. Circ Res, 1983, 53: 502–514
6 Wang C, Chen X, Wang L, *et al.* Bioadhesive ultrasound for long-term continuous imaging of diverse organs. Science, 2022, 377: 517–523
7 Palombo C, Kozakova M. Arterial stiffness, atherosclerosis and cardiovascular risk: Pathophysiologic mechanisms and emerging clinical indications. Vascular Pharmacol, 2016, 77: 1–7
8 Blackshear WM, Phillips DJ, Chikos PM, *et al.* Carotid artery velocity patterns in normal and stenotic vessels.. Stroke, 1980, 11: 67–71
9 Neyra NR, Ikizler TA, May RE, *et al.* Change in access blood flow over time predicts vascular access thrombosis. Kidney Int, 1998, 54: 1714–1719
10 Kenny JES, Munding CE, Eibl JK, *et al.* A novel, hands-free ultrasound patch for continuous monitoring of quantitative Doppler in the carotid artery. Sci Rep, 2021, 11: 1–11
11 Gao X, Chen X, Hu H, *et al.* A photoacoustic patch for three-dimensional imaging of hemoglobin and core temperature. Nat Commun, 2022, 13: 7757
12 Hu H, Huang H, Li M, *et al.* A wearable cardiac ultrasound imager. Nature, 2023, 613: 667–675
13 Stock KF, Klein B, Steubl D, *et al.* Comparison of a pocket-size ultrasound device with a premium ultrasound machine: diagnostic value and time required in bedside ultrasound examination. Abdom Imag, 2015, 40: 2861–2866
14 Tanter M, Fink M. Ultrafast imaging in biomedical ultrasound. IEEE Trans Ultrason Ferroelect Freq Contr, 2014, 61: 102–119
15 Baribeau Y, Sharkey A, Chaudhary O, *et al.* Handheld point-of-care ultrasound probes: The new generation of POCUS. J Cardiothoracic Vascular Anesth, 2020, 34: 3139–3145
16 Wang Z, Xue QT, Chen YQ, *et al.* A flexible ultrasound transducer array with micro-machined bulk PZT. Sensors, 2015, 15: 2538–2547
17 Hu H, Zhu X, Wang C, *et al.* Stretchable ultrasonic transducer arrays for three-dimensional imaging on complex surfaces. Sci Adv, 2018, 4: eaar3979
18 Liu W, Chen W, Zhu C, *et al.* Design and micromachining of a stretchable two-dimensional ultrasonic array. Micro Nano Eng, 2021, 13: 100096
19 Pashaei V, Dehghanzadeh P, Enwia G, *et al.* Flexible body-conformal ultrasound patches for image-guided neuromodulation. IEEE Trans Biomed Circuits Syst, 2020, 14: 305–318
20 Dussik KT. Über die Möglichkeit, hochfrequente mechanische Schwingungen als diagnostisches Hilfsmittel zu verwerten. Z f d g Neur u Psych, 1942, 174: 153–168
21 Satomura S. Ultrasonic Doppler method for the inspection of cardiac functions. J Acoust Soc Am, 1957, 29: 1181–1185
22 Jaffe B, Roth RS, Marzullo S. Piezoelectric properties of lead ceramics. J Appl Phys, 1954, 809: 10–12
23 Smith SW, Pavy HG, von Ramm OT. High-speed ultrasound volumetric imaging system. I. Transducer design and beam steering. IEEE Trans Ultrason Ferroelect Freq Contr, 1991, 38: 100–108
24 von Ramm OT, Smith SW, Pavy HG. High-speed ultrasound volumetric imaging system. II. Parallel processing and image display. IEEE Trans Ultrason Ferroelect Freq Contr, 1991, 38: 109–115
25 Klicker KA, Biggers JV, Newnham RE. Composites of PZT and epoxy for hydrostatic transducer applications. J Am Ceramic Soc, 1981, 64: 5–9
26 Savakus HP, Klicker KA, Newnham RE. PZT-epoxy piezoelectric transducers: A simplified fabrication procedure. Mater Res Bull, 1981, 16: 677–680
27 Wang C, Qi B, Lin M, *et al.* Continuous monitoring of deep-tissue haemodynamics with stretchable ultrasonic phased arrays. Nat Biomed Eng, 2021, 5: 749–758
28 Wang C, Li X, Hu H, *et al.* Monitoring of the central blood pressure waveform *via* a conformal ultrasonic device. Nat Biomed Eng, 2018, 2: 687–695
29 Wang F, Jin P, Feng Y, *et al.* Flexible Doppler ultrasound device for the

 © Science China Press 2024

monitoring of blood flow velocity. Sci Adv, 2021, 7: eabi9283
30 Bjaerum S, Torp H, Kristoffersen K. Clutter filters adapted to tissue motion in ultrasound color flow imaging. IEEE Trans Ultrason Ferroelect Freq Contr, 2002, 49: 693–704
31 Rizzatto G. Ultrasound transducers. Eur J Radiol, 1998, 27: S188–S195
32 Goll JH. The design of broad-band fluid-loaded ultrasonic transducers. IEEE Trans Son Ultrason, 1979, 26: 385–393
33 Park JH, Lee SM, Park J, *et al.* Acoustic matching layer films using B-stage thermosetting polymer resins for ultrasound transducer applications. IEEE Trans Ultrason Ferroelect Freq Contr, 2020, 67: 2148–2154
34 Szabo TL. Doppler modes. In: Diagnostic Ultrasound Imaging. Amsterdam: Elsevier, 2004, 337–380
35 Zwiebel WJ, Pellerito JS. Introduction to vascular ultrasonography. In: SA Carter (ed). Hemodynamic considerations in peripheral vascular and cerebrovascular disease. Amsterdam: Elsevier, 2005, 3–17
36 Abe K, Iwanaga H, Shimada Y, *et al.* The effect of nicardipine on carotid blood flow velocity, local cerebral blood flow, and carbon dioxide reactivity during cerebral aneurysm surgery. Anesth Analg, 1993, 76: 1227–1233
37 Maulik D. Spectral Doppler sonography: Waveform analysis and hemodynamic interpretation. In: Doppler ultrasound in obstetrics and gynecology: 2nd revised and enlarged edition. Berlin/Heidelberg: Springer-Verlag, 2005, 4: 35–36
38 Azhim A, Katai M, Akutagawa M. Exercise improved age-associated changes in the carotid blood velocity waveforms. J Biomed, 2007, 1: 17–26
39 Demeulenaere O, Sandoval Z, Mateo P, *et al.* Coronary flow assessment using 3-dimensional ultrafast ultrasound localization microscopy. JACC-Cardiovasc Imag, 2022, 15: 1193–1208

Acknowledgements This work was supported by the Minstry of Science and Technology (2022YFA1203001, 2022YFA1203002 and 2023YFC2410900), the National Natural Science Foundation of China (T2321003, 22335003, T2222005 and 22175042) and Science & Technology Commission of Shanghai Municipality (21511104900, 20JC1414902 and 23490713500). The authors would like to thank Professors Jiayan Dai and Jiaming Zhang from the Department of Applied Physics of Hong Kong Polytechnic University for the simulation study of pulse-echo performance and impedance/phase spectrum and helpful discussion.

Author contributions Xu K and Peng H conceived the idea. Zou J, Guo X and Wu J designed the experiments. Zou J wrote the original draft. Chen P and Zou J participated in the design and layout of the pictures and reviewed the manuscript. Xu K and Chen P supervised the work, reviewed and revised the manuscript. All authors contributed to the general discussion.

Conflict of interest The authors declare that they have no conflict of interest.

Supplementary information Experimental details and supporting data are available in the online version of the paper.

Junyi Zou is a PhD candidate in Prof. Huisheng Peng's group at Fudan University. His current research interests mainly focus on the design of high-performance flexible and weavable ultrasonic transducers.

Xingyi Guo received his BE degree in electronic information science and technology from Fudan University in 2021. He is currently a postgraduate at the Department of Biomedical Engineering, Fudan University. His research interests include signal processing, medical ultrasound imaging and super resolution ultrasound localization microscopy.

Kailiang Xu received his PhD degree in biomedical engineering from Fudan University in 2012. He is currently an associate professor at the Department of Biomedical Engineering, Fudan University. His research interests include wave simulation, signal processing, inverse problems, the development of multiwave imaging techniques, and elasticity characterization for medical ultrasound and nondestructive evaluation.

Peining Chen is currently a professor at the Department of Macromolecular Science and Laboratory of Advanced Materials, Fudan University. He received BS, MS, and PhD degrees from Sichuan University (2010), Sun Yat-sen University (2012) and Fudan University (2016), respectively. He then worked as a postdoctoral fellow at the Department of Electrical and Computer Engineering, University of Toronto before joining Fudan University in 2017. His research focuses on new flexible electronic materials and devices.

Huisheng Peng is currently a professor at the Department of Macromolecular Science and Laboratory of Advanced Materials, Fudan University. He received his BS degree in polymer materials from Donghua University in 1999, MS degree in macromolecular chemistry and physics from Fudan University in 2003, and PhD degree in chemical engineering from Tulane University, USA in 2006. He then worked at Los Alamos National Laboratory before joining Fudan University in 2008. His research centers on the new direction of fiber electronics.

可编织、可穿戴的宽带聚合物超声换能器

邹君逸[1†], 郭星奕[2†], 吴家琦[1], 徐冬梅[2], 许凯亮[2*], 陈培宁[1*], 他得安[2], 彭慧胜[1*]

摘要 新兴的物联网技术推动了可穿戴健康监测设备的快速发展. 目前, 医学超声技术在严重慢性疾病的长时间监测方面具有广阔的应用前景. 然而, 商用超声探头一般都是刚性的, 需要手持, 难以满足医疗可穿戴设备对柔性化、小型化和舒适性的要求. 本文提出了一种可编织、可穿戴的聚合物超声换能器, 该换能器由匹配层、背衬层和压电层组成. 聚合物压电材料的带宽(93%)是压电陶瓷的7倍, 并且可以承受超过10,000次的弯曲和扭曲变形. 该传感器能监测颈动脉血液流速, 心脏血液流速和心脏血管的血管厚度, 并具有与商用探头相当的信噪比. 它的宽带特性(3.68–10.08 MHz)使其能通过调整频率来监测不同的组织. 可编织超声换能器可以制成纤维形式, 并编织成透气织物, 在不牺牲穿戴舒适性的情况下进行实时血管监测.

 © Science China Press 2024